From gravity cores to overpressure history: the importance of measured sediment physical properties in hydrogeological models

Davide Mencaroni[1]*, Jaume Llopart[1], Roger Urgeles[1], Sara Lafuerza[2], Eulàlia Gràcia[1], Anne Le Friant[3] and Morelia Urlaub[4]

[1]Institut de Ciències del Mar (CSIC), 08003 Barcelona, Spain

[2]Sorbonne Université, Paris, 75006 France

[3]Institut de Physique du Globe de Paris, 75005 Paris, France

[4]GEOMAR Helmholtz Centre for Ocean Research Kiel, 24148 Kiel, Germany

DM, 0000-0002-4736-7526; JL, 0000-0002-9495-1194; RU, 0000-0001-9438-1753; SL, 0000-0003-2126-6505; EG, 0000-0001-9311-3108; ALF, 0000-0001-8901-2515; MU, 0000-0002-1116-636X

*Correspondence: mencaroni@icm.csic.es

Abstract: The development of overpressure in continental margins is typically evaluated with hydrogeological models. Such approaches are used to both identify fluid flow patterns and to evaluate the development of high pore pressures within layers with particular physical properties that may promote slope instability. In some instances, these models are defined with sediment properties based on facies characterization and proxy values of porosity; permeability or compressibility are derived from the existing literature as direct measurements are rarely available. This study uses finite-element models to quantify the differences in computed overpressure generated by fine-grained hemipelagic sediments from the Gulf of Cadiz, offshore Martinique and the Gulf of Mexico, and their consequences in terms of submarine slope stability. By comparing our simulation results with *in situ* pore pressure data measured in the Gulf of Mexico, we demonstrate that physical properties measured on volcanic-influenced hemipelagic sediments underestimate the computed stability of a submarine slope. Physical properties measured on sediments from the study area are key to improving the reliability and accuracy of overpressure models, and when that information is unavailable, literature data from samples with similar lithologies, composition and depositional settings enable better assessment of the overpressure role as a pre-conditioning factor in submarine landslide initiation.

Overpressure development in marine sediments is a major pre-conditioning factor that favours slope instability by decreasing the amount of gravitational driving stresses required to mobilize sediments (Dugan and Sheahan 2012). If the pressure of the water contained in the pore space exceeds the hydrostatic condition, failures can be initiated in low-angle submarine slopes by a relatively minor trigger such as a small magnitude earthquake (Urlaub *et al.* 2015). Generation of overpressure is commonly associated with rapid sedimentation (Dickinson 1953; Gibson 1958) and with the physical properties of the sediments, such as porosity, hydraulic conductivity and compressibility. The occurrence of overpressure within sediments can be studied directly through *in situ* measurements with piezocone tests (Lunne *et al.* 1997) and pore pressure penetrometers (Flemings *et al.* 2008), or indirectly from borehole logging measurements, such as sonic, resistivity and density logs (Mouchet and Mitchelle 1989), and from velocity analysis derived from seismic reflection data. Finally, overpressure development and evolution can be evaluated using hydrogeological models. The application at the basin scale of those models, in some cases, aims to provide a broad understanding of the conditions that may have generated previous slope instability (Gutierrez and Wangen 2005; Bellwald *et al.* 2019; Llopart *et al.* 2019). In many cases, however, sediment samples from the study area are not available for geotechnical testing. In such instances, porosity, permeability and compressibility values are typically derived from the literature based on their expected lithologies (Urlaub *et al.* 2015), depositional environment (Bellwald *et al.* 2019) or geographical area. On the other hand, measuring sediments' physical properties implies a series of inevitable errors and uncertainties, which affect the reliability of models, such as the presence of test errors, an insufficient number of tests and the inherent variability of

From: Georgiopoulou, A., Amy, L. A., Benetti, S., Chaytor, J. D., Clare, M. A., Gamboa, D., Haughton, P. D. W., Moernaut, J. and Mountjoy, J. J. (eds) 2020. *Subaqueous Mass Movements and their Consequences: Advances in Process Understanding, Monitoring and Hazard Assessments*. Geological Society, London, Special Publications, **500**, 289–300. First published online May 22, 2020, https://doi.org/10.1144/SP500-2019-176

soil properties (Phoon and Kulhawy 1999; Zhang *et al.* 2012).

This study aims to evaluate the suitability of hydrogeological models based on literature-derived physical properties of sediments collected from similar depositional environments and with comparable grain-size distributions. To do this, we built a series of finite-element models that simulate the development of overpressure on a hemipelagic unit rapidly buried by a series of mass wasting events. Using the same depositional scenario, we defined the hemipelagic layer with initial porosity, hydraulic conductivity and specific storage measured on comparable sediments with similar grain-size distribution, but collected in three different depositional settings: Alentejo Basin (Gulf of Cadiz, SW Iberian margin), Grenada Basin (offshore Martinique, Lesser Antilles) and Ursa Basin (Gulf of Mexico). We further used the actual sedimentary history at Ursa Basin, where overpressure is ground-truthed with piezometer measurements, and tested the influence of using actual physical properties from the area v. physical properties taken from other depositional environments of similar grain size.

Depositional settings

We based this study on mechanical properties from 18 hemipelagic sediment samples collected from three different oceanic regions, characterized by different depositional settings, and all affected by well-documented subaqueous slope instabilities (Fig. 1a). The Alentejo Basin is located in the northern sector of the Gulf of Cadiz, SW offshore Portugal (Fig. 1b). The area is characterized by an extensive contourite depositional system (Hernández-Molina *et al.* 2015), generated by the Mediterranean Outflow Water, which distributes sediments entering the gulf mainly through the Guadalquivir river (Mulder *et al.* 2003). The Grenada Basin (Fig. 1c), offshore Martinique, is mainly composed of volcanic ashes, hemipelagic sediments and volcanoclastic turbidite deposits (Lafuerza *et al.* 2014) due to the activity of the surrounding volcanoes and absence of important sediment inputs from rivers. The sediments in the deep part of the basin accumulate at sedimentation rates up to 20 cm a^{-1} (Le Friant *et al.* 2015). The third area is the Ursa Basin (Fig. 1d), in the Gulf of Mexico. The region is known for the very high terrigenous sedimentation, entering the basin

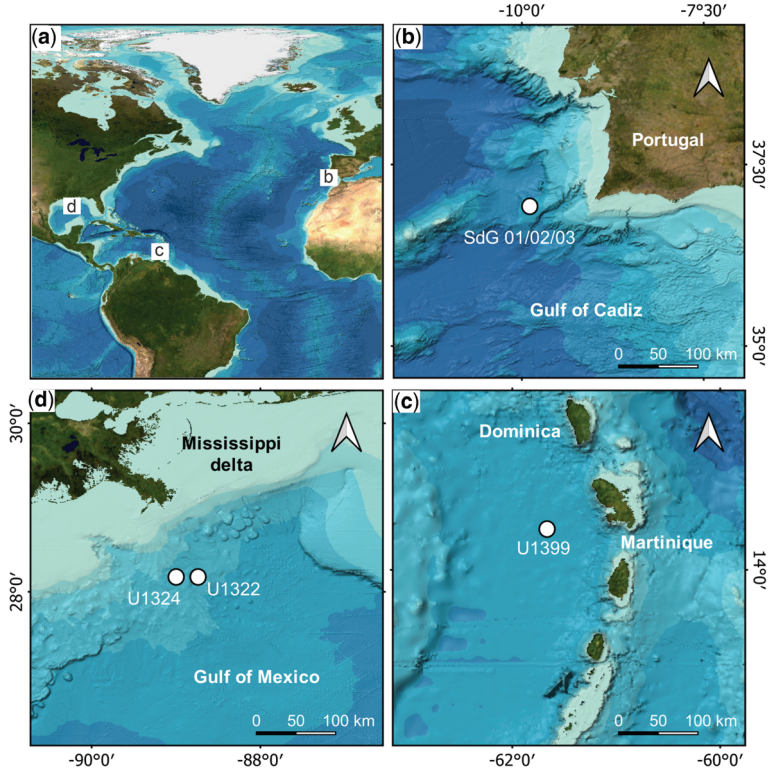

Fig. 1. (**a**) Location of the areas where the sediments considered in this study were collected. Detailed location of the cores in the (**b**) Alentejo Basin, (**c**) Grenada Basin and (**d**) Ursa Basin.

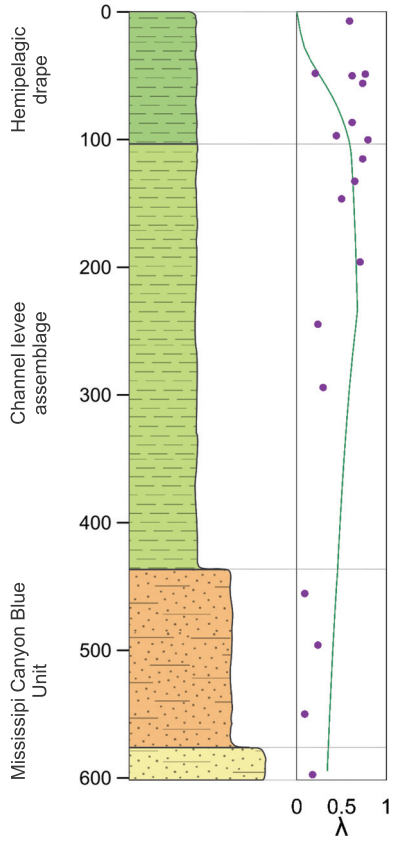

Fig. 2. Site U1324 stratigraphic model adopted for the 1D simulation with corresponding overpressure: *in situ* piezometer overpressure measurements (purple dots) (Expedition 308 Scientists 2005); reference 1D modelling result (green line) (Urgeles *et al.* 2010). Properties for overpressure models in Figure 7 are only changed for the upper hemipelagic drape.

from the Mississippi River, taking place upon a salt substrate (Worrall and Snelson 1989). The slope is characterized by well-documented overpressure due to sedimentation rates exceeding 25 m ka^{-1} during some intervals in the Pleistocene (Flemings *et al.* 2006; Sawyer *et al.* 2007). IODP Expedition 308 performed *in situ* pore pressure measurements using the DVTPP and T2P piezoprobes (see Flemings *et al.* 2008; Long *et al.* 2008 for further details on the measurements), and documented high overpressure associated mainly with the high sedimentation rates in the area (Expedition 308 Scientists 2005). Previous studies (Urgeles *et al.* 2007, 2010) modelled the stratigraphic evolution of the margin considering the physical properties of the different units in the Ursa Basin, with the aim of understanding the present-day pore pressure condition revealed by the *in situ* measurements. Despite the significant scatter observed in the direct overpressure measurement, especially within the uppermost hemipelagic drape, 1D simulations reproduced the general vertical overpressure distribution at site U1324 (Fig. 2) (for more information about previous overpressure modelling, see Urgeles *et al.* 2010).

Methods

Sediments from the Alentejo Basin (six samples) have been collected using a gravity corer during the INSIGHT_Leg1 (2018) cruise in the Gulf of Cadiz. Initial void ratio (e_0), compression index (C_c) and initial hydraulic conductivity (k_0) in these samples have been derived with stepped loading (Rowe and Barden type of cell) or Constant Rate of Strain (CRS) oedometer tests (Fig. 3a and Table 1). Samples from the Grenada Basin (three samples) and from the Ursa Basin (nine samples) were recovered from wells drilled during two separate IODP expeditions. The samples from the Grenada Basin used in this study were drilled at well U1399 during the IODP expedition 340 (Le Friant *et al.* 2015) and their compressibility/permeability properties measured with 1D consolidation tests (Fig. 3b) (Lafuerza *et al.* 2014). Sediments from the Ursa Basin were taken from wells U1322 and U1324, drilled during the IODP Expedition 308 (Expedition 308 Scientists 2005; Flemings *et al.* 2006). Their physical properties were also analysed using a combination of incremental loading and CRS oedometer tests (Fig. 3c) (Urgeles *et al.* 2007, 2010; Long *et al.* 2008; Stigall and Dugan 2010).

In our basin-modelling approach, we input the physical properties of the sediments at their initial depositional conditions, to simulate the pre-failure overpressure behaviour of the sediment composing the stratigraphic column. Therefore, input data such as porosity, hydraulic conductivity and specific storage are extrapolated to 1 kPa along the virgin consolidation line (e.g. Llopart *et al.* 2019). All of the samples were composed of hemipelagic sediments, collected outside mass transport deposit areas: for this reason, we assumed they did not undergo heavy deformation or mixing processes and the extrapolation of their physical properties to 1 kPa can be considered as a fair reproduction of their behaviour at depositional conditions.

Grain-size distribution for all samples was measured using laser diffractometers. We adopted the grain-size classification proposed by Wentworth (1922) to derive the percentages of sand (2 mm–62.5 μm), silt (62.5–4 μm) and clay (<4 μm) measured in the sediments. The three-component textural classification for muddy sediments proposed by Flemming (2000) was used to subdivide the analysed sediments into four classes based on their sand, silt

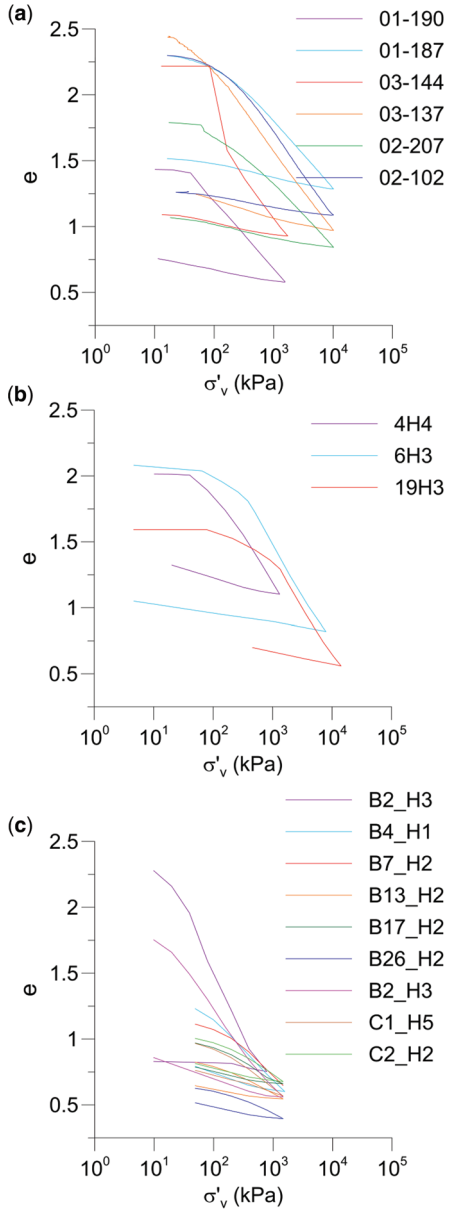

Fig. 3. Consolidation curves showing void ratio e reduction while increasing uniaxial loading σ'_v. Each plot refers to one of the analysed areas: (**a**) Alentejo Basin; (**b**) Grenada Basin (Lafuerza *et al.* 2014); (**c**) Ursa Basin (Urgeles *et al.* 2010).

and clay content: D-II (very silty, slightly sandy mud), D-III (silty, slightly sandy mud), E-II (slightly clayey silt) and E-III (clayey silt) (Fig. 4).

Overpressure development simulations were performed using the finite element software BASIN (Bitzer 1996, 1999). Modelling the stratigraphic and hydrodynamic evolution of a 2D section, BASIN allows the calculation of non-equilibrium compaction and overpressure generation on sediments by coupling compaction and 2D fluid flow. The consolidation model incorporates porosity-dependent sediment compressibility through equation (1) (Bitzer 1996):

$$\left(\frac{\partial}{\partial x}\frac{k_{x(\phi)}\partial p}{\partial x}\right)+\left(\frac{\partial}{\partial x}\frac{k_{z(\phi)}\partial p}{\partial z}\right)=\frac{(1-\phi)\rho g\alpha_{(\phi)}\partial p}{\partial t} \quad (1)$$

where $k_{x(\phi)}$ is the porosity-dependent hydraulic conductivity in the x-direction, $\alpha_{(\phi)}$ is the porosity-dependent sediment compressibility, p the fluid pressure, ϕ the porosity, ρ is the sediment bulk density, g is the gravity constant, t is the time (s) and z is depth (m). Sediment compressibility in BASIN is calculated from the specific storage (S_s), which is defined as the volume of water removed from a unit volume of a confined aquifer with an increase in the vertical stress. It relates to the more commonly used compression index by the relation (Jorgensen 1980):

$$S_s=\frac{0.434C_c\gamma_w}{\sigma'_v(1+e_0)} \quad (2)$$

where C_c is the compression index, γ_w is the specific weight of water, σ'_v is the effective vertical stress and e_0 is the void ratio at depositional conditions (1 kPa).

In the first instance, we built a series of 1D models to simulate the deposition of a 500 m thick hemipelagic unit with a sedimentation rate of 30 cm a^{-1}, followed by a series of turbidite events that deposit 250 m of sand-rich material during 1000 years. Initial thickness of the units, sedimentation rates and boundary conditions, as well as physical properties of the turbidite unit, are kept constant through the different scenarios. Since no samples associated with turbidites were available in our database, we defined its physical properties with values taken from the literature (Reed *et al.* 2002). The only variables that change between the different models are initial porosity, initial hydraulic conductivity and initial specific storage of the hemipelagic layer. In the first set of analyses (Scenario A), we defined the properties of the hemipelagic unit by averaging arithmetically the values of the physical properties for each study area. In the second series of tests (Scenario B), we assigned physical properties to each hemipelagic layer based on the average specific storage, porosity and hydraulic conductivity of the samples from each grain-size class. The BASIN input parameters used for the simulation are provided in Table 2.

Secondly, to evaluate the reliability of our results and their significance in terms of submarine slope stability, we applied our approach on a case study where *in situ* overpressure measurements have been collected. To do so, we considered the results

Table 1. *Compiled physical and grain-size data from the Gulf of Cadiz, Martinique and the Gulf of Mexico*

Area	Sample	Original depth (mbsf)	Sand (%)	Silt (%)	Clay (%)	Texture class*	ϕ_0	C_c	k_0
Alentejo Basin	SdG-01_190	1.9	4.93	57.36	37.71	E-III	0.69	0.52	1.57×10^{-8}
	SdG-01_187	1.8	3.57	62.58	33.85	E-III	0.76	0.50	2.45×10^{-8}
	SdG-03_144	1.4	0.7	69.89	29.41	E-III	0.74	0.48	5.25×10^{-8}
	SdG-03_137	1.3	1.66	70.32	28.28	E-III	0.77	0.62	6.22×10^{-8}
	SdG-02_207	2.0	8.49	66.23	25.28	D-III	0.72	0.45	2.31×10^{-8}
	SdG-02_102	1.0	0.24	61.25	38.51	E-III	0.78	0.65	7.87×10^{-8}
Ursa Basin	308_1322_B2_H3	8.0	0	57.8	42.2	E-III	0.77	0.92	5.70×10^{-10}
	308_1322_B4_H1	24.0	0	68	32	E-III	0.71	0.57	1.12×10^{-8}
	308_1322_B7_H2	54.0	8.2	62.2	29.6	D-III	0.66	0.41	3.48×10^{-8}
	308_1322_B13_H2	111.0	0	68.1	31.9	E-III	0.56	0.23	1.06×10^{-8}
	308_1322_B17_H2	144.0	0	61.69	38.4	E-III	0.59	0.25	3.08×10^{-8}
	308_1322_B26_H2	212.0	0.63	73.37	26	E-III	0.52	0.22	4.41×10^{-8}
	308_1324_B2_H3	8.0	2.65	72.4	24.4	E-II	0.71	0.58	2.32×10^{-8}
	308_1324_C1_H5	57.0	0	74.3	25.7	E-III	0.63	0.35	8.87×10^{-9}
	308_1324_C2_H2	103.0	0	79.8	20.2	E-II	0.61	0.28	5.70×10^{-10}
Grenada Basin	340-1399B_4H4	30.5	10.5	75.8	13.7	D-II	0.78	0.69	1.55×10^{-9}
	340-1399B_6H3	46.5	3.9	76.1	20.1	E-II	0.79	0.75	1.32×10^{-9}
	340-1399B_19H3	138.9	5.8	83.1	11.1	D-II	0.77	0.67	1.41×10^{-9}

ϕ_0, initial porosity; C_c, compression index; k_0, initial hydraulic conductivity (m s^{-1}).
*Flemming (2000).

of site U1324 drilled in the Ursa Basin during IODP Expedition 308.

Using BASIN, we reproduced the stratigraphic architecture, sedimentation rate, boundary conditions and lithologies of a 1D overpressure model at site U1324 from Urgeles *et al.* (2010) (Fig. 2). Then, we substituted the original physical properties associated with the top hemipelagic drape with those measured from the sediments collected in the Alentejo and Grenada basins (Table 2). By doing this, we aim to evaluate the differences in overpressure generated by defining hydrogeological models with physical properties measured from hemipelagic sediments collected in different areas, and compare them with the reference calibrated results from Urgeles *et al.* (2010). At site U1324, 612 m of sedimentary sequence deposited between the Pleistocene and the Holocene (Expedition 308 Scientists 2005; Flemings *et al.* 2008) were drilled. From bottom to top, the main units composing the Ursa Basin consist of: (1) the sand-dominated lower Mississippi Canyon Blue Unit (Late Pleistocene) (Sawyer *et al.* 2007), (2) a mud-dominated channel levee assemblage and (3) a mud drape deposited during the last *c.* 20 ka (Behrmann *et al.* 2006; Flemings *et al.* 2008). The overpressure evolution of the basin has been modelled and is modelled in this study since deposition of the sand-rich Blue unit (*c.* 100 ka ago), followed by the silt lithologies associated with the filling of the Ursa Canyon, and by the mud-dominated sediments from the channel levee assemblage and hemipelagic sediments (Fig. 2) (Urgeles *et al.* 2007, 2010).

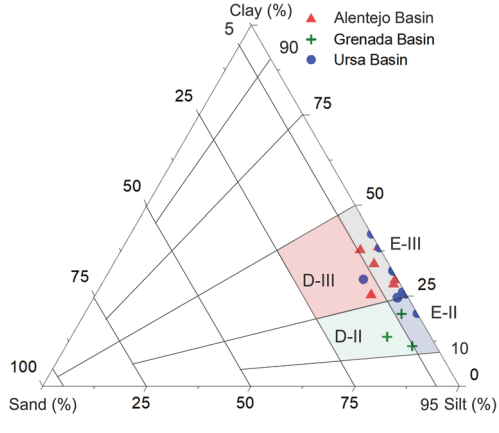

Fig. 4. Grain-size distribution of the sediments analysed for this study. The internal subdivision refers to the classification for muddy marine sediments proposed by (Flemming 2000) and adopted in this work.

This study also refers to pore pressure in terms of the overpressure ratio (λ) (Flemings *et al.* 2008), defined as:

$$\lambda = \frac{(p - p_h)}{(\sigma_v - p_h)} \quad (3)$$

where p is pore pressure, p_h is the hydrostatic pressure and σ_v is the lithostatic or total vertical stress.

Table 2. *Parameters used for the simulations in BASIN*

	Samples	Initial porosity	Initial specific storage (m^{-1})	Initial hydraulic conductivity ($m\ s^{-1}$)
Turbidite layer	(Urgeles *et al.* 2010)	0.5	0.001	1×10^{-6}
Hemipelagic	Alentejo Basin	0.74	0.025	4.28×10^{-8}
Scenario A – areas	Grenada Basin	0.78	0.005	1.43×10^{-9}
	Ursa Basin	0.64	0.023	2.71×10^{-8}
Hemipelagic	D-II	0.77	0.003	1.48×10^{-9}
Scenario B – classes	D-III	0.69	0.014	2.90×10^{-8}
	E-II	0.70	0.017	1.04×10^{-7}
	E-III	0.69	0.027	3.09×10^{-8}

The physical properties associated with the turbidity layer were used in all the simulations, while the hemipelagic changed.

A λ value of 0 means that pore pressure is hydrostatic, while a value of 1 means that the overburden is fully sustained by the pore water.

Results

Physical properties

The grain-size distribution of sediments collected in each study area is relatively homogeneous although each location has a distinctly different composition. Whilst all samples analysed are silt dominated, the percentages vary significantly between 57.36 and 83.1%. Clay contents also ranged between 11.1 and 42.2%, and sand-sized grains comprised the lowest fraction at each site (0 to 10.5%) (Fig. 4). The Ursa Basin has the lowest sand content, with 8 out of 9 samples corresponding to the 'E' class of Flemming's classification (sand <5%). Within the Grenada Basin, 2 out of 3 samples tested show a sand content greater than 5% and a clay content less than 25%. Sediments from the Alentejo Basin are similar to the Ursa Basin: sand content is less than 5% for 5 out of 6 samples, with clay values between 25 and 35%. Therefore, group D-II in Flemming's classification is represented by only two samples from the Ursa Basin.

We used ternary contour diagrams to visualize the different textural composition of sediments in relation to their compression index (Fig. 5a), initial porosity (Fig. 5b) and initial hydraulic conductivity (Fig. 5c). Results show a broadly heterogeneous relationship between grain size and physical properties. The compression index (Fig. 5a) ranges between 0.22 and 0.92. The highest C_c values are related to an increase in silt percentage and tend to decrease in sediments with some sand content. Samples from the Grenada Basin, with higher silt content, show a compression index ranging between 0.67 and 0.75, while the lowest values are found in sediments from the Ursa Basin, where most of the samples show C_c values below 0.65. An exception is represented

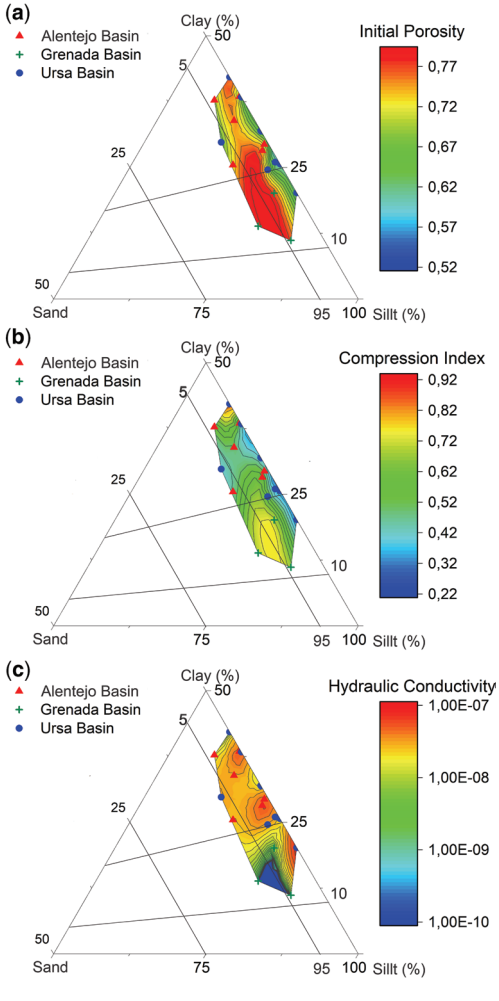

Fig. 5. Ternary contour diagrams comparing sediment composition (% sand, silt and clay) with (**a**) initial porosity, (**b**) compression index and (**c**) hydraulic conductivity. Sand axes have been reduced to the range 50–100% to facilitate visualization.

by sample 308-1322B_H08, which has higher clay content (42.2%) and compression index (0.92).

A similar trend is illustrated in the initial porosity diagram (Fig. 5b), with porosity values ranging between 0.52 and 0.79. The higher values are reached in sediments with higher silt content while the lower values are linked to higher sand content. However, sample SdG_02_102 differs from this trend, showing a high initial porosity (0.78) despite a relatively low silt content (61%).

Values of hydraulic conductivity at deposition (1 kPa) vary within two orders of magnitude (10^{-8} to 10^{-10} m s^{-1}). The Alentejo Basin samples produce the highest values while the lowest values correspond to samples from the Grenada Basin (Fig. 5c).

Our first modelling stage (Scenario A) (Fig. 6a) consisted of three separate models, where the physical properties of the hemipelagic layer described above were averaged for each study area (Table 2). Fine-grained sediments from the Alentejo Basin and from the Ursa Basin show a comparable range of overpressure development, reaching a maximum overpressure ratio (λ) of 0.18 at 343 mbsf for the Alentejo Basin model and 0.25 at 341 mbsf for the Ursa Basin (i.e. immediately below the turbidite unit). The computed overpressure ratio from the Grenada Basin model shows higher values, with λ up to 0.56 at 329 mbsf.

The second modelling scenario (Scenario B) consisted of defining the hemipelagic units with physical properties averaged from their grain-size distribution classes (Fig. 6b). The minimum peak value ($\lambda \sim 0.06$) is observed in the model defined with properties from group E-II (sand <5%, clay <25%). Models from groups E-III and D-III show comparable maximum overpressure ratios (0.24 and 0.19), while the maximum values ($\lambda \sim 0.53$) are reached by the model defined with the properties averaged from the samples in group D-II (sand >5%, clay <25%).

Figure 7 shows the present-day overpressure resulting at site U1324 from our 1D simulations.

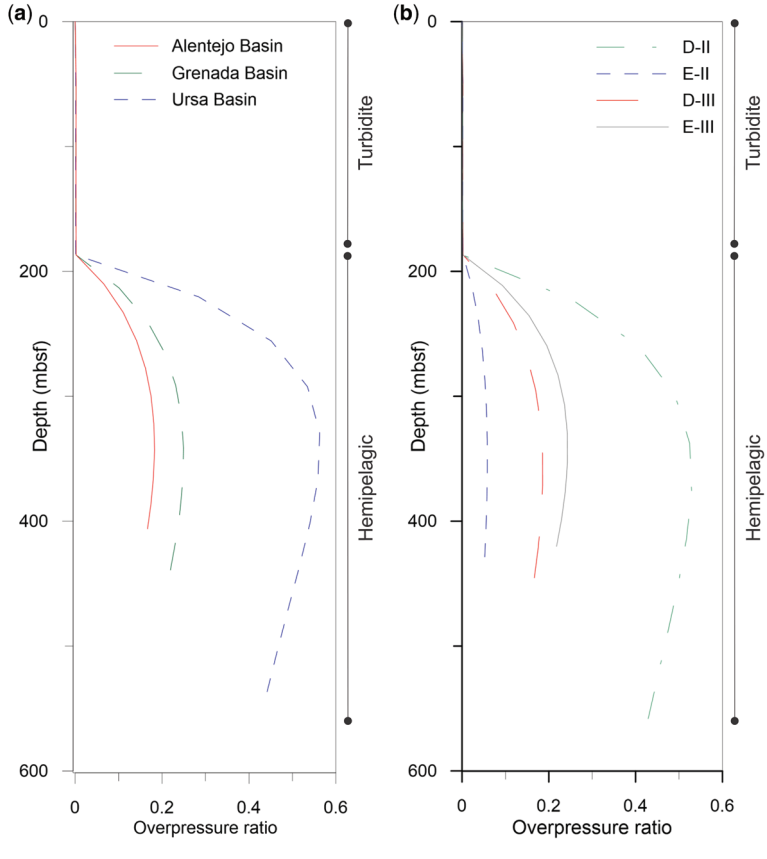

Fig. 6. Overpressure generated at the end of the simulations v. computed final depths. The plots refer to (**a**) Scenario A, where physical properties of the hemipelagic units are averaged from each study area and (**b**) Scenario B, where the properties of the hemipelagic layer are averaged from each of the four represented textural classes.

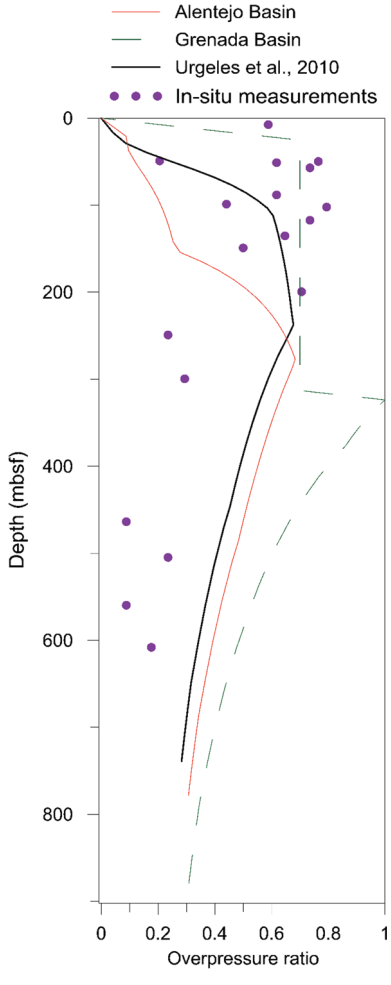

Fig. 7. Overpressure generated at site U1324 v. the computed final depth for the (1) *in situ* piezometer measurements (purple dots); reference overpressure modelled at the same site by Urgeles *et al.* (2010) (black line); overpressure resulting by defining the hemipelagic units with properties collected from the other study areas (red and green lines).

Changes in the physical properties of the hemipelagic unit, at the top of the stratigraphy, did not allow any of our scenarios to fit perfectly either with the reference 1D model (Urgeles *et al.* 2010) or the *in situ* overpressure measurements (Flemings *et al.* 2008). The model defined with hydraulic conductivity, specific storage and initial porosity from the Alentejo Basin underestimates the overpressure within the hemipelagic layer, mainly because of its higher permeability compared with the hemipelagic sediment from the Ursa Basin (Table 2). Finally, the model defined with physical properties from the Grenada Basin provides a very different output compared with the other models (Fig. 7). Even if it reproduces the measured *in situ* overpressures from the hemipelagic layer more effectively, the hydrodynamics of the model are split into two separate systems: in the lower part of the stratigraphy the overpressure increases constantly from the bottom to the top, reaching a maximum overpressure value of 1 at the base of the muddy sediments. Above this point, the overpressure drops, keeping a constant value of 0.7 up to the seafloor.

Discussion

In the first part of our study, two different scenarios were used to analyse the influence of variable grain-size composition of hemipelagic sediments in overpressure development. In Scenario (A), the hemipelagic layer was defined using physical properties collected from specific study areas and resulted in much higher overpressure generation for sediments of the Grenada Basin compared to the other two areas considered. In Scenario (B), the samples with relatively high silt and low clay content and sand content higher than 5% (sediment class D-II) generated the highest overpressure. This sediment class includes only two samples, both collected in the Grenada Basin. In this case, the results obviously coincide with those of samples for the Grenada Basin in Scenario A. Our results therefore seem to show that overpressure generation is rather related to the sediment composition and depositional setting instead of grain-size distribution. This is in agreement with previous studies showing that there is no direct correlation between grain-size distribution and sediment physical properties (Lafuerza *et al.* 2014) in marine muddy sediments.

However, when considering each depositional environment (e.g. river influenced), the grain-size distribution has a major influence on overpressure development. Thus, sediments with low clay content (E-II) and samples with similar clay content but higher sand content (D-III) generated lower overpressure (Figs 4 and 6a). Nonetheless, factors not considered in this study, such as sorting and particle rounding, might have played a significant role that should be investigated in future work.

Comparing the overpressure results with the physical properties used for the simulations indicates that the development of overpressure is associated with low initial hydraulic conductivities and specific storage (Table 2). Such differences in the physical properties between the Grenada Basin and the other two areas could reflect substantial diversity in sediment composition and mineralogy. This may, in turn, be directly linked to the depositional

environment: (a) the hemipelagic sediments in the Alentejo and Ursa basins are largely fluvially derived from the Guadalquivir and Mississippi rivers, respectively; (b) volcanically derived sediments from the Grenada Basin are influenced by volcanic ash released by the extensive series of volcanos in the Lesser Antilles volcanic arc (Wiemer and Kopf 2015).

Comparing the 1D consolidation behaviour for volcanically derived hemipelagic sediments to the river-fed samples, it is possible to make assumptions about the reason for such notable differences in physical properties (Fig. 3). The Grenada Basin sediments show lower compressibility at low consolidation stress and a transition to high compressibility at higher vertical stress (Fig. 3b). Similar behaviour known as structuration has been documented especially for fossiliferous, cemented or highly bioturbated sediments (Locat *et al.* 2003; Spinelli *et al.* 2007): in these instances, sediments are capable of holding water in rigid structures, preventing compaction during the early stages of consolidation or, in the case of high degrees of cementation, also at high burial depths. Physical properties of the sediments from the Grenada Basin, with higher compression index and lower specific storage and hydraulic conductivity, suggest that a similar mechanism could occur in the volcanic ash-rich hemipelagic sediments from the Lesser Antilles volcanic arc. Volcanic ashes, in fact, may generate the same type of structures that prevent porewater being released into the system at low consolidation stresses.

Structuration in the Grenada Basin sediments retains the water in the pore space, reducing the specific storage (which is, by definition, the volume of water removed from a unit volume of a confined aquifer) and decreasing the permeability, since the porewater gets trapped in the rigid structures. Those physical properties represent the ideal conditions for the development of overpressure in marine sediments, and this could explain why the Grenada Basin sediments (Scenario A) develop higher overpressure (near lithostatic), which leads to a lower vertical displacement in the model.

It must be also mentioned that defining hydrogeological models with marine sediments that show structuration might question the hydrogeological model results. 'Delayed consolidation' (Locat *et al.* 2003), as seen in the Grenada Basin hemipelagic sediments (Fig. 3b), implies two different consolidation responses within the same sediment sample. Considering that the compression index is usually input as one representative value for each lithology, modelling such variation can represent a challenge. This is the reason why it is important to recognize structuration phenomena in the analysed samples and to consider their consequences while evaluating simulation results.

This behaviour is well exemplified when modelling the Ursa Basin sedimentation history with physical properties from the Grenada Basin (Fig. 7). The lower hydraulic conductivity and specific storage of the sediments from the Grenada Basin, mainly due to the structuring phenomena previously discussed, make the hemipelagic unit act as a perfectly impermeable seal in the case of the very high sedimentation rates of the Ursa Basin. The porewater from the lower formations, characterized by coarser grain size and higher permeability, flows upwards and accumulates at the base of the seal, reaching extreme overpressure values up to 1 (Fig. 7). Nonetheless, this trend does not find correspondence in the *in situ* measurement, where overpressure reaches its maximum within the hemipelagic layer and decreases constantly with depth, indicating a continuity between the porewater flow in the lower part of the stratigraphy and in the uppermost hemipelagic layer.

Significance for submarine slope stability

The development of overpressure in a submarine slope affects the magnitude of the events that can trigger a failure (e.g. earthquakes), or, in case of very high values and/or steep slope, can lead to slope instability with no external trigger (Stigall and Dugan 2010; Urlaub *et al.* 2015). A preliminary quantification of the consequences from the different overpressure resulting from our 1D models at site U1324 can be made by calculating the factor of safety (FoS) on a hypothetical 2° submarine slope using equation (4) (Flemings *et al.* 2008):

$$\mathrm{FoS} = \frac{\tan \phi_{\mathrm{f}}}{\sin \theta \cos \theta}(\cos^2 \theta - \lambda) \qquad (4)$$

where θ is the surface slope, λ the overpressure ratio and θ_{f} the friction angle of 28° as it was measured on the hemipelagic sediments in the Ursa Basin (Urgeles *et al.* 2007). FoS greater than 1 indicates a stable slope, while values lower than 1 indicate slope failure.

The FoS was calculated on the sediment deposited starting from 40 ka ago, corresponding to the beginning of the mud-dominated channel levee assemblage, until the present day (Fig. 8). As the FoS decreases with increasing overpressure, the model generated defining the hemipelagic units with the physical properties from the Alentejo and the original Ursa Basin reference model shows a decrease in the factor of safety until 20 ka. At this point, the hemipelagic sediment starts depositing and porewater migrates upwards with overpressure dissipating towards the seafloor (Fig. 8). The FoS for these two models reaches a minimum of around 3, increasing up to 5 at the present day. In contrast,

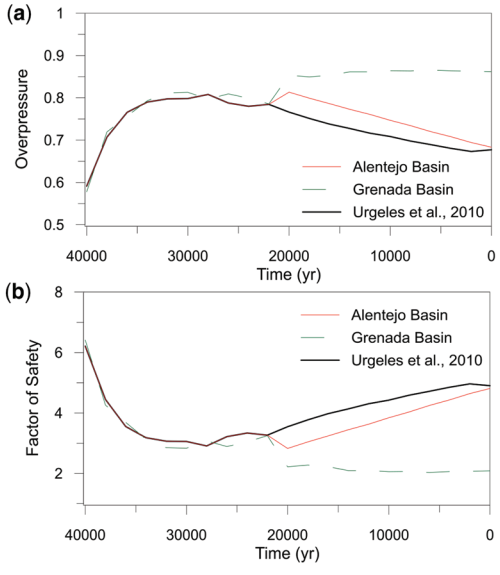

Fig. 8. (**a**) Overpressure evolution during the last 40 ka and (**b**) computed factor of safety for all models at the location of IODP Site U1324. The graph refers to the base of the fine-grained channel levee assemblage unit, which started depositing around 40 ka ago.

the model where the hemipelagic layer is defined with the physical properties from the Grenada Basin shows an increase in overpressure values also after 20 ka. This is because the deposition and compaction of the hemipelagic sediments creates a seal that prevents the water from the lower part of the stratigraphy flowing upwards. In this case, the FoS reaches values of around 2, which propagate almost constantly from 20 ka until the present day (Fig. 8).

At the end of the simulations, none of the models results in a FoS low enough to induce the slope to fail (<1) in the considered stratigraphic level. Nevertheless, 1D sedimentation models at site U1324 show a completely different overpressure development history when the model is defined with the hemipelagic sediments from the Grenada Basin, resulting in a considerable underestimation of the FoS at the base of the first deposited fine sediment unit.

Our modelling results show that physical properties derived from only the lithological characterization or the grain-size distribution available in the literature may produce inaccurate overpressure models, with consequent misleading slope stability estimations. On the other hand, models based on physical properties derived from similar grain size, depositional environment and expected compositional nature of sediments, such as the ones from the Alentejo Basin and the Ursa Basin, provided similar overpressure development results. This indicates that, in the absence of direct measurements, literature-derived physical properties based on grain-size characteristics and depositional setting are expected to produce more accurate overpressure development for stability analysis of submarine slopes. However, care should be taken in settings where the presence of microfossils such as diatoms, initial cementation or volcanic glass particles could provide sediment structuration.

Conclusions

Using hydrogeological modelling we show how the sediment characteristics in some depositional environments have a significant influence on the amount of overpressure generated in marine hemipelagic sediments. We demonstrate how fine-grained marine sediments collected from different sedimentary environments (volcanic-influenced v. river-dominated) can result in differences in overpressure in excess of one order of magnitude and discuss the consequences of those discrepancies for submarine slope stability assessment. Phenomena, such as structuration of marine sediments, need to be carefully considered when carrying out basin hydrogeological models. Our results support the idea that, to achieve accurate results, besides accurate stratigraphic architecture and age of units, hydrogeological models should be defined with physical properties measured from samples collected in the study area. In instances where such an approach is not feasible, assigning an initial void ratio, hydraulic conductivity and specific storage extracted from the literature for samples with similar expected lithologies, composition and depositional settings are likely to provide the most accurate estimates. Given that the data are generally difficult to find within the scientific literature, a global open database for published physical properties is paramount to increase the accuracy of basin hydrogeological models in the future.

Acknowledgements This research used samples and/or data provided by the International Ocean Discovery Program (IODP). We also thank Brandon Dugan and another reviewer for their comments that significantly improved our manuscript.

Funding Davide Mencaroni was supported by a Marie Skłodowska-Curie Doctoral Fellowship through the SLATE Innovative Training Network within the European Union Framework Programme for Research and Innovation Horizon 2020 under Grant Agreement No. 721403. The Spanish 'Ministerio de Economia y Competitividad' and the European Regional Development Fund through grant CTM2015-70155-R (project INSIGHT) are also acknowledged.

Author contributions **DM**: conceptualization (lead), data curation (lead), formal analysis (lead), writing – original draft (lead), writing – review & editing (lead); **JL**: data curation (supporting), formal analysis (equal), methodology (lead), supervision (lead), validation (equal), visualization (equal), writing – original draft (supporting), writing – review & editing (supporting); **RU**: conceptualization (supporting), data curation (supporting), formal analysis (supporting), methodology (equal), supervision (equal), visualization (supporting), writing – original draft (supporting), writing – review & editing (equal); **SL**: data curation (supporting), resources (supporting); **EG**: resources (supporting); **ALF**: resources (supporting); **MU**: conceptualization (supporting), methodology (supporting).

References

Behrmann, J.H., Flemings, P.B. *et al*. 2006. Rapid sedimentation, overpressure, and focused fluid flow, Gulf of Mexico continental margin. *Scientific Drilling*, **1**, 12–17, https://doi.org/10.2204/iodp.sd.3.03.2006

Bellwald, B., Urlaub, M., Hjelstuen, B.O., Sejrup, H.P., Sørensen, M.B., Forsberg, C.F. and Vanneste, M. 2019. NE Atlantic continental slope stability from a numerical modeling perspective. *Quaternary Science Reviews*, **203**, 248–265, https://doi.org/10.1016/j.quascirev.2018.11.019

Bitzer, K. 1996. Modeling consolidation sedimentary and fluid basins flow. *Computers and Geosciences*, **22**, 467–478, https://doi.org/10.1016/0098-3004(95)00113-1

Bitzer, K. 1999. Two-dimensional simulation of clastic and carbonate sedimentation, consolidation, subsidence, fluid flow, heat flow and solute transport during the formation of sedimentary basins. *Computers and Geosciences*, **25**, 431–447, https://doi.org/10.1016/S0098-3004(98)00147-2

Dickinson, G. 1953. Geological aspects of abnormal reservoir pressures in Gulf Coast Louisiana. *AAPG Bulletin*, **37**, 410–432.

Dugan, B. and Sheahan, T.C. 2012. Offshore sediment overpressures of passive margins: mechanisms, measurement, and models. *Reviews of Geophysics*, **50**, 271–276, https://doi.org/10.1029/2011RG000379

Expedition 308 Scientists 2005. *Overpressure and fluid flow processes in the deepwater Gulf of Mexico: slope stability, seeps, and shallow-water flow*. Integrated Ocean Drilling Program Expedition 308 Scientific Prospectus. IODP Publications.

Flemings, P., Behrmann, J. and John, C. and Expedition 308 Scientists 2006. *Proceedings of the Ocean Drilling Program*. IODP Management International, Inc., College Station TX.

Flemings, P.B., Long, H., Dugan, B., Germaine, J., John, C.M., Behrmann, J.H. and Sawyer, D. 2008. Pore pressure penetrometers document high overpressure near the seafloor where multiple submarine landslides have occurred on the continental slope, offshore Louisiana, Gulf of Mexico. *Earth and Planetary Science Letters*, **274**, 269–283, https://doi.org/10.1016/j.epsl.2008.06.027

Flemming, B.W. 2000. A revised textural classification of gravel-free muddy sediments on the basis of ternary diagrams. *Continental Shelf Research*, **20**, 1125–1137, https://doi.org/10.1016/S0278-4343(00)00015-7

Gibson, R.E. 1958. The progress of consolidation in a clay layer increasing in thickness with time. *Géotechnique*, **8**, 171–182, https://doi.org/10.1680/geot.1958.8.4.171

Gutierrez, M. and Wangen, M 2005. Modeling of compaction and overpressuring in sedimentary basins. *Marine and Petroleum Geology*, **22**, 351–363, https://doi.org/10.1016/j.marpetgeo.2005.01.003

Hernández-Molina, F.J., Sierro, F.J. *et al*. 2015. Evolution of the gulf of Cadiz margin and southwest Portugal contourite depositional system: Tectonic, sedimentary and paleoceanographic implications from IODP expedition 339. *Marine Geology*, **377**, 7–39, https://doi.org/10.1016/j.margeo.2015.09.013

Jorgensen, D.G. 1980. *Relationships between Basic Soils-Engineering Equations and Basic Ground-Water Flow Equations*. Geological Survey Water-Supply Paper 2064. US Department of the Interior.

Lafuerza, S., Le Friant, A. *et al*. 2014. Geomechanical characterization of submarine volcano-flank sediments, Martinique, Lesser Antilles Arc. *In*: Krastel, S., Behrmann, J.-H. *et al*. (eds) *Submarine Mass Movements and their Consequences: 6th International Symposium*. Springer, Cham, 73–81, https://doi.org/10.1007/978-3-319-00972-8_7

Le Friant, A., Ishizuka, O. *et al*. 2015. Submarine record of volcanic island construction and collapse in the Lesser Antilles arc: first scientific drilling of submarine volcanic island landslides by IODP Expedition 340. *Geochemistry Geophysics Geosystems*, **16**, 420–442, https://doi.org/10.1002/2014GC005684.Key

Llopart, J., Urgeles, R. *et al*. 2019. Fluid flow and pore pressure development throughout the evolution of a trough mouth fan, western Barents Sea. *Basin Research*, **31**, 487–513, https://doi.org/10.1111/bre.12331

Locat, J., Tanaka, H., Tan, T., Dasari, G.R. and Lee, H.J. 2003. Natural soils: geotechnical behavior and geological knowledge. *In*: Tan, T., Phoon, K., Hight, D. and Leroueil, S. (eds) *Characterisation and Engineering Properties of Natural Soils*. Swets & Zeitlinger, The Netherlands, 3–28.

Long, H., Flemings, P.B., Germaine, J.T., Saffer, D.M. and Dugan, B. 2008. Data report: consolidation characteristics of sediments from IODP Expedition 308, Ursa Basin, Gulf of Mexico. *Proceedings of the Integrated Ocean Drilling Program*, **308**, https://doi.org/10.2204/iodp.proc.308.204.2008

Lunne, T., Robertson, P.K. and Powell, J.J.M. 1997. *Cone Penetration Testing in Geotechnical Practice*. Spon-Press, London.

Mouchet, J.P. and Mitchelle, A. 1989. *Abnormal Pressures While Drilling – Origins, Prediction, Detection, Evaluation. Manuals Techniques 2*. Elf Aquita, Boussens.

Mulder, T., Voisset, M. *et al*. 2003. The Gulf of Cadiz: an unstable giant contouritic levee. *Geo-Marine Letters*, **23**, 7–18, https://doi.org/10.1007/s00367-003-0119-0

Phoon, K.-K. and Kulhawy, F.H. 1999. Characterization of geotechnical variability. *Canadian Geotechnical Journal*, **36**, 612–624, https://doi.org/10.1139/t99-038

Reed, A.H., Briggs, K.B. and Lavoie, D.L. 2002. Porometric properties of siliciclastic marine sand: a comparison of traditional laboratory measurements with image

analysis and effective medium modeling. *IEEE Journal of Oceanic Engineering*, **27**, 581–592, https://doi.org/10.1109/JOE.2002.1040940

Sawyer, D.E., Flemings, P.B., Shipp, R.C. and Winker, C.D. 2007. Seismic geomorphology, lithology, and evolution of the late Pleistocene Mars–Ursa Turbidite region, Mississippi Canyon Area, Northern Gulf of Mexico. *AAPG Bulletin*, **91**, 215–234, https://doi.org/10.1306/08290605190

Spinelli, G.A., Mozley, P.S., Tobin, H.J., Underwood, M.B., Hoffman, N.W. and Bellew, G.M. 2007. Diagenesis, sediment strength, and pore collapse in sediment approaching the Nankai Trough subduction zone. *Geological Society of America Bulletin*, **119**, 377–390, https://doi.org/10.1130/B25920.1

Stigall, J. and Dugan, B. 2010. Overpressure and earthquake initiated slope failure in the Ursa region, northern Gulf of Mexico. *Journal of Geophysical Research*, **115**, B04101, https://doi.org/10.1029/2009JB006848

Urgeles, R., Locat, J. and Dugan, B. 2007. Recursive failure of the Gulf of Mexico continental slope: timing and causes. *In*: Lykousis, V., Sakellariou, D. and Locat, J. (eds) *Submarine Mass Movements and Their Consequences*. Springer, Dordrecht, 209–219, https://doi.org/10.1007/978-1-4020-6512-5_22

Urgeles, R., Locat, J., Sawyer, D.E., Flemings, P.B., Dugan, B. and Binh, N.T.T. 2010. History of pore pressure build up and slope instability in mud-dominated sediments of Ursa Basin, Gulf of Mexico Continental Slope. *In*: Mosher, D.C., Shipp, R.C., Moscardelli, L., Chaytor, J.D., Baxter, C.D.P., Lee, H.J. and Urgeles, R. (eds) *Submarine Mass Movements and Their Consequences*. Springer, Dordrecht, 179–190, https://doi.org/10.1007/978-90-481-3071-9_15

Urlaub, M., Talling, P.J., Zervos, A. and Masson, D.G. 2015. What causes large submarine landslides on low gradient sediment accumulation? *Journal of Geophysical Research: Solid Earth*, **120**, 1–18, https://doi.org/10.1002/2015JB012347.

Wentworth, C.K. 1922. A scale of grade and class terms for clastic sediments. *The Journal of Geology*, **30**, 377–392, https://doi.org/10.1086/622910

Wiemer, G. and Kopf, A. 2015. Altered marine tephra deposits as potential slope failure planes? *Geo-Marine Letters*, **35**, 305–314, https://doi.org/10.1007/s00367-015-0408-4

Worrall, D.M. and Snelson, S. 1989. Evolution of the northern Gulf of Mexico, with emphasis on Cenozoic growth faulting and the role of salt. *In*: Bally, A.W. and Paler, A.R. (eds) *The Geology of North America – An Overview*, Vol. **A**. Geological Society of America, Boulder, CO.

Zhang, J., Tang, W.H., Zhang, L.M. and Huang, H.W. 2012. Characterising geotechnical model uncertainty by hybrid Markov Chain Monte Carlo simulation. *Computers and Geotechnics*, **43**, 26–36, https://doi.org/10.1016/j.compgeo.2012.02.002